



Isogeometric dual reciprocity boundary element method for solving transient heat conduction problems with heat sources

Bo Yu^{a,b,*}, Geyong Cao^a, Wendong Huo^c, Huanlin Zhou^a, Elena Atroshchenko^b

^a School of Civil Engineering, Hefei University of Technology, Hefei 230009, PR China

^b School of Civil and Environmental Engineering, University of New South Wales, Sydney, NSW 2052, Australia

^c State Key Laboratory of Structural Analysis for Industrial Equipment, Dalian University of Technology, Dalian 116023, PR China

ARTICLE INFO

Article history:

Received 30 May 2020

Received in revised form 29 July 2020

Keywords:

Isogeometric BEM

Dual reciprocity BEM

NURBS basis functions

Transient heat conduction problems

ABSTRACT

Up to now, the isogeometric boundary element method (IGBEM) has been widely applied in different fields, and the solved problems are basically independent of time. But an excellent numerical method is more than that, so it is necessary to explore a new IGBEM which can solve time-domain problems. Based on this, the isogeometric dual reciprocity boundary element method (IG-DRBEM) is proposed to solve transient heat transfer problems with heat sources. The introduction of the dual reciprocal method enables the IGBEM to solve the transient heat transfer problem conveniently. At the same time, it does not need to divide elements within the domain, which maintains the advantage of the IGBEM. First, the boundary domain integral equation is established by the weighted residual method and the field variables are discretized by NURBS basis functions. Then, the domain integral in the integral equation is transformed into the boundary by the classical dual reciprocity method. Finally, the standard first-order ordinary differential equations are formed. In order to examine the accuracy of the proposed method, several typical numerical examples are discussed carefully. The presented method can provide a new idea for solving time-dependent problems by IGBEM.

© 2020 Elsevier B.V. All rights reserved.

1. Introduction

The boundary element method (BEM) was introduced several decades ago as a highly accurate numerical method for solving boundary integral equations. The main advantage of the BEM in comparison with the finite element (FEM) and other domain type methods is the fact, that in absence of body forces the governing equations are formulated on the boundary only and therefore only discretization of the boundary is required. According to the division of time, the development of BEM can be roughly classified as the three stages such as the tradition BEM, the BEM that solving large-scale problems such as the fast multipole BEM, and the presented isogeometric BEM (IGBEM) stage.

The BEM has been successfully applied to a wide range of problems. Earlier studies include crack problems [1], water wave problems [2], electromagnetic field problems [3], dynamic analysis [4], thermo-fluids and acoustics field problems [5]. Although the dimensionality of the problem in the BEM is reduced by one in comparison with the FEM and less degrees of freedom are required to achieve the same accuracy of the solution, the computational cost of the

* Corresponding author at: School of Civil Engineering, Hefei University of Technology, Hefei 230009, PR China.
E-mail address: yubochina@hfut.edu.cn (B. Yu).

BEM is often higher than that of the FEM. High computational cost is associated with the properties of the main matrix, which in the BEM is dense and non-symmetric, even the computation process will be interrupted for the large scale problem. Fortunately, the emergence of the fast multipole BEM makes the BEM possible to solve large-scale problems [6,7]. Many BEM researchers adopted the fast multipole expansion technique to solve the three-dimensional crack problems [8], the potential problems [9], the three-dimensional acoustic wave problems [10], the rigid-inclusion problems of carbon nanotubes [11] and others. The fast multipole BEM can be regarded as the promotion of the computational speed and solving scale by means of the fast multipole expansion scheme. In addition, the adaptive cross approximation [12] is also the common acceleration method. To some extent, the introduction of these acceleration methods also expands the application scope of BEM.

However, all of these studies need to convert the CAD model into suitable elements for numerical analysis. Generally, the pre-processing may take up the majority of the analysis time. Based on this, in 2005, the iso-geometric analysis (IGA) was proposed by Hughes et al. [13] with the aim to use Computer-Aided Design (CAD) geometries directly for numerical analysis. Geometries in CAD are parameterized by spline basis functions which can be used as shape functions to discretize the weak form in the FEM or the integral equation in the BEM (approach known as IGBEM). Recently, someone introduced the idea of isogeometric analysis into other methods and formed many new numerical methods such as the isogeometric collocation method [14], the isogeometric meshless finite volume method [15], the scaled boundary isogeometric finite element method [16,17] with transient heat transfer [18]. First implementation of IGBEM with NURBS was demonstrated in [19] for 2D elasticity. Then in 2013, Scott et al. [20] developed IGBEM by using unstructured T-splines. Further, Peake et al. [21] proposed the extended isogeometric boundary element method (XIBEM) to solve the two-dimensional Helmholtz problem. To solve the large-scale problem, Takahashi and Matsumoto [22] introduced the fast multipole method (FMM) into IGBEM for Laplace equation. Recently, Chen et al. [23] applied the isogeometric fast multipole boundary element method to solve the 2D half-space acoustic scattering problems. Dolz et al. [24] proposed the fast IGBEM based on the FMM to analyze three-dimensional electromagnetic scattering problems.

In general, the coefficient matrix generated by the boundary element method is asymmetric. However, the symmetric Galerkin boundary element method (SGBEM) [25] can generate symmetric coefficient matrix, which can save calculation cost to some extent. In 2016, the isogeometric SGBEM (IG-SGBEM) has been proposed to solve the Laplace problem [26] and the crack problem [27]. Recently, Aimi et al. [28] based on B-splines adopted the IG-SGBEM to analyze 2D elliptic model problems.

More recently, Peng et al. [29] applied IGBEM to analyze three-dimensional static fracture and fatigue crack growth problems. Gong et al. [30] developed IGBEM to solve three-dimensional potential problems, where the calculation of singular integral is detailedly discussed. In 2018, An et al. [31] utilized the IGBEM to analyze the two-dimensional steady heat transfer problem. Generally, NURBS can be used to accurately describe the geometric shape and only a few degrees of freedom are needed, especially for the unknown quantities of BEM, so IGBEM can easily solve the shape optimization problems. As mentioned the paper from Lian et al. [32], there is no need for mesh generation and CAD model recovery when the shape optimization is carried out by IGBEM. Because the optimization variable is coordinates of control points, the entity model of the optimization object or the production of the product can be directly carried out at the end of the shape optimization. In addition, IGBEM is also adopted to optimize the shape of the structure in three-dimensional acoustic problems [33]. In 2020, Sun et al. [34] and Wu et al. [35] adopted IGBEM to solve the 3D elastic inclusion problems and the 3D acoustic problem, respectively. Fang et al. [36] used IGBEM with the time-dependent fundamental solution to analyze the transient heat transfer problem. Beer et al. [37] published a book about IGBEM, which involves many extensive aspects, such as the establishment of boundary integral equations, the basic knowledge of IGA, the extraction of geometric information of CAD and some applications of IGBEM.

It has been nearly 15 years since the development of IGA, and many open source code of IGAFEM and IGBEM have emerged [38] such as open source C++ IGA library Gismo [39], an open source IGA Matlab code was described in [40] with a restriction to 2D scalar PDEs. An excellent open source IGA code was written in Matlab [41]. An object-oriented C++ combining IGA with FEM code was discussed in [42]. An IGABEM code written in Matlab was introduced in [43]. An C++ library (Bembel) featuring higher order isogeometric Galerkin boundary element methods for Laplace, Helmholtz, and Maxwell problems was presented in [44].

Note that these problems analyzed by the above IGBEM basically belong to time independent. A valuable numerical method should not be limited to the analysis of steady-state problems. In this paper, the transient heat transfer problem will be solved by IGBEM.

IGBEM is known for high accuracy due to the exact representation of the boundary geometry by splines, and it also inherits all main features of the BEM. However, some major challenges limit application of the BEM to a narrow class of problems. One of the challenges is associated with the presence of domain integrals in problems with sources or time terms. In such cases, the volume or surface mesh needs to be created and the approach loses its advantage of being the "boundary-only". Therefore, it is desired to transform domain integrals into the equivalent boundary integrals. Based on this, many scholars proposed some effective transformation methods of domain integrals. For example, in 1982, Nardini and Brebbia [45,46] introduced firstly the dual reciprocity method (DRM) into BEM and formed the famous dual reciprocity BEM (DRBEM). The emergence of DRBEM makes it possible for BEM to analyze various transient or nonlinear

problems [47]. Up to now, DRBEM has been widely used to solve the nonlinear diffusion problem [48], the dynamic analysis [49], the thermal wave propagation in biological tissues [50], the anisotropic dynamic crack problem [51], the magneto-thermo-viscoelastic problems of rotating functionally graded anisotropic plates [52], the axisymmetric thermoelastostatic analysis of nonhomogeneous materials [53], the transient heat transfer problem [54–57], the coupled burgers' equations [58], the elastoplastic problem [59] and so on. After 20 years of proposing DRBEM method, in 2002, another famous domain integral transformation method which is called as the radial integration method (RIM) was proposed by Gao [60]. Coupling RIM and BEM to form the radial integration BEM (RIBEM), up to now, RIBEM has been widely used to solve dynamic problems of anisotropic plates [61], heat conduction problems [62–64], Fracture analysis of functionally graded materials [65], dynamic coupled thermoelastic problems [66], one-phase solidification problems [67] and so on. RIM adopts the pure mathematical treatments to transform domain integrals into boundary integrals. However, the approximate processes of the two domain integral transformation methods for solving some problems are similar. For example, the unknown function term is approximated by radial basis functions. Compared with RIM, DRM is easier to implement and operate. Also, DRBEM has been realized in the famous BEM business software BEASY. In this work, we couple DRM with IGBEM (approach abbreviated as IG-DRBEM) for problems of transient heat conduction with heat sources. To the authors' knowledge, up to date, it is the first implementation of IG-DRBEM in the literature.

The paper is organized as follows. The B-spline and NURBS functions are described in Section 2. The definition of problem is introduced in Section 3. The isogeometric dual reciprocity BEM is elaborated in Section 4. Then, several numerical examples are discussed in Section 5. Finally, the main findings of the present work are summarized in Section 6.

2. Non-Uniform Rational B-Splines (NURBS)

NUBRS are commonly used in CAD to describe curves and surfaces. Here we briefly recall the main definitions. First, a knot vector is defined as a non-decreasing sequence of coordinates in the parametric space:

$$\mathcal{E} = \{\xi_1, \xi_2, \dots, \xi_{n+p+1}\} \tag{1}$$

where n and p denote the number and the degree of the basis functions. Typically, an open knot vector is assumed, for which knots ξ_1 and ξ_{n+p+1} are repeated $p + 1$ times. Non-zero knot spans $[\xi_i, \xi_{i+1}]$ are referred to as elements. B-Splines basis functions $N_{a,p}(\xi)$ are defined recursively as follows:

$$N_{a,0} = \begin{cases} 1 & \xi_a \leq \xi < \xi_{a+1} \\ 0 & \text{otherwise} \end{cases} \tag{2}$$

and for $p \geq 1$

$$N_{a,p}(\xi) = \frac{\xi - \xi_a}{\xi_{a+p} - \xi_a} N_{a,p-1}(\xi) + \frac{\xi_{a+p+1} - \xi}{\xi_{a+p+1} - \xi_{a+1}} N_{a+1,p-1}(\xi) \tag{3}$$

NURBS are defined as

$$R_{a,p}(\xi) = \frac{N_{a,p}(\xi) w_a}{\sum_{i=1}^n N_{i,p}(\xi) w_i} \tag{4}$$

where w_i is the weight associated with the i th basis function. If all weights are equal, NUBRS reduce to B-Splines. Therefore, B-Splines are considered as a special case of NURBS.

NURBS curve $\mathbf{x}(\xi) = (x(\xi), y(\xi))$, defined by n control points $\mathbf{x}_a = (x_a, y_a)$, is parameterized as follows:

$$\mathbf{x}(\xi) = \sum_{a=1}^n R_{a,p}(\xi) \mathbf{x}_a \tag{5}$$

3. Problem definition

In what follows, we consider a two-dimensional bounded domain Ω ($\Omega \in \mathbb{R}^2$) with boundary $\Gamma = \partial\Omega$, occupied by the isotropic material with constant material parameters. The governing equation for transient heat conduction can be expressed as

$$k\nabla^2 T(\mathbf{x}, t) + g(\mathbf{x}, t) = \rho c \frac{\partial T(\mathbf{x}, t)}{\partial t}, \quad \mathbf{x} \in \Omega \tag{6}$$

where $\mathbf{x} = (x_1, x_2)$ is a generic point in Ω , ∇^2 is the Laplace operator, $T(\mathbf{x}, t)$ is the temperature at the point \mathbf{x} at time t , $g(\mathbf{x}, t)$ is a known heat source function, k is the thermal conductivity, ρ is the density and c is the specific heat.

The initial condition is given by

$$T(\mathbf{x}, 0) = T_0(\mathbf{x}) \tag{7}$$

where $T_0(\mathbf{x})$ is a prescribed function. In this paper, two types of boundary conditions are considered, namely

$$T(\mathbf{x}, t) = \bar{T}(\mathbf{x}, t), \quad \mathbf{x} \in \Gamma_1 \tag{8}$$

and

$$-k \frac{\partial T}{\partial n} = \bar{q}(\mathbf{x}, t), \quad \mathbf{x} \in \Gamma_2 \tag{9}$$

where $\Gamma_1 \cup \Gamma_2 = \Gamma$, $\Gamma_1 \cap \Gamma_2 = \emptyset$, n is a unit outward normal to Γ , $\bar{T}(\mathbf{x}, t)$ and $\bar{q}(\mathbf{x}, t)$ are the prescribed temperature and the heat flux histories on the corresponding parts of the boundary, respectively.

4. Isogeometric dual reciprocity BEM

To some extent, the introduction of IGBEM theory can be divided into two parts. One is the introduction of conventional boundary integral equation and giving the discretized forms. The other part is to replace the original shape function with NUBRS basis functions. Similarly, we will introduce firstly the DRBEM theory, then, adopt NURBS basis functions to discretize the boundary integral equation with DRBEM.

4.1. Dual reciprocity boundary integral equation

To facilitate the use of dual reciprocity method, Eq. (6) is first rewritten as

$$\nabla^2 T(\mathbf{x}, t) = b(T(\mathbf{x}, t), \mathbf{x}, t) \tag{10}$$

where

$$b(T(\mathbf{x}, t), \mathbf{x}, t) = \frac{1}{\lambda} \frac{\partial T(\mathbf{x}, t)}{\partial t} - \frac{g(\mathbf{x}, t)}{k} \tag{11}$$

in which $\lambda = k/\rho c$. The right hand side of Eq. (10) is subsequently approximated by a set of N_t functions $\{f_j(\mathbf{x})\}_{j=1}^{N_t}$ and the corresponding time-dependent coefficients $\{\alpha_j(t)\}_{j=1}^{N_t}$ as

$$b(T(\mathbf{x}, t), \mathbf{x}, t) = \sum_{j=1}^{N_t} \alpha_j(t) f_j(\mathbf{x}) \tag{12}$$

where for each function $f_j(\mathbf{x})$ there exists a function $\hat{T}_j(\mathbf{x})$ such that $\nabla^2 \hat{T}_j(\mathbf{x}) = f_j(\mathbf{x})$. Various choices of functions $f_j(\mathbf{x})$ have been investigated in the literature [45]. In this work, we adopt the polynomial function of distance $r_j = \|\mathbf{x} - \mathbf{x}_j\|$ to point \mathbf{x}_j inside or on the boundary of domain Ω :

$$f_j(\mathbf{x}) = 1 + r_j + r_j^2 + \dots + r_j^m \tag{13}$$

Then

$$\hat{T}_j(\mathbf{x}) = \frac{r_j^2}{4} + \frac{r_j^3}{9} + \dots + \frac{r_j^{m+2}}{(m+2)^2} \tag{14}$$

In what follows, we will also need

$$\hat{q}_j(\mathbf{x}) = \frac{\partial \hat{T}_j(\mathbf{x})}{\partial n} = \left(r_{x_1} \frac{\partial x_1}{\partial n} + r_{x_2} \frac{\partial x_2}{\partial n} \right) \left(\frac{1}{2} + \frac{r_j}{3} + \dots + \frac{r_j^m}{m+2} \right) \tag{15}$$

where r_{x_1} and r_{x_2} are the x_1 - and x_2 -components of r_j .

Eq. (10) can be multiplied by the fundamental solution of steady state heat conduction problems T^* and integrated over the domain, producing

$$\int_{\Omega} (\nabla^2 T(\mathbf{x}, t)) T^* d\Omega = \sum_{j=1}^{N_t} \alpha_j(t) \int_{\Omega} (\nabla^2 \hat{T}_j(\mathbf{x})) T^* d\Omega \tag{16}$$

where $T^* = \frac{1}{2\pi} \ln\left(\frac{1}{r}\right)$ in 2D, $r = \|\mathbf{x} - \mathbf{x}'\|$.

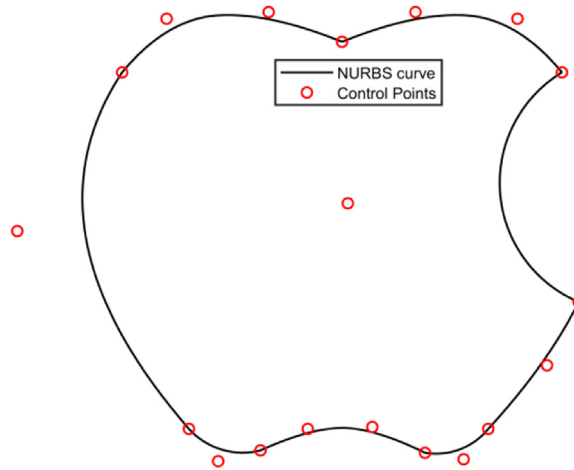


Fig. 1. The domain created using NURBS.

Table 1
Element connectivity information.

Number of element	Node 1	Node 2	Node 3
1	1	2	3
2	3	4	5
3	4	5	6
4	6	7	8
5	7	8	9
6	9	10	11
7	11	12	13
8	13	14	15
9	14	15	16
10	16	17	18
11	18	19	1

Integrating Eq. (16) by parts, for any source point $\mathbf{x}' \in \Gamma$, the integral equation without domain integrals is derived

$$\begin{aligned}
 & C(\mathbf{x}')T(\mathbf{x}', t) + \int_{\Gamma} T(\mathbf{x}, t)q^*(\mathbf{x}', \mathbf{x})d\Gamma - \int_{\Gamma} q(\mathbf{x}, t)T^*(\mathbf{x}', \mathbf{x})d\Gamma \\
 &= \sum_{j=1}^{N_t} \alpha_j(t) \left[C(\mathbf{x}')\hat{T}_j(\mathbf{x}') + \int_{\Gamma} \hat{T}_j(\mathbf{x})q^*(\mathbf{x}', \mathbf{x})d\Gamma - \int_{\Gamma} \hat{q}_j(\mathbf{x})T^*(\mathbf{x}', \mathbf{x})d\Gamma \right]
 \end{aligned} \tag{17}$$

where $C(\mathbf{x}')$ is a jump term in which it can be obtained similar to the conventional BEM [46], q^* is the normal derivative of which along the boundary Γ and $q^* = \partial T^*/\partial \mathbf{n}$.

Eq. (17) is the governing dual reciprocity boundary integral equation for the transient heat problem, which will be subsequently discretized by the NUBRS basis functions. Note that Eq. (17) does not involve any domain integrals. However, it involves N_t points, which define functions $\hat{T}_j(\mathbf{x})$ and $\hat{q}_j(\mathbf{x})$, and which can be distributed on the boundary and inside the domain.

4.2. Isogeometric approximation

Similar to the conventional BEM, we need to define the boundary element first. In IGBEM, the unique values contained in the knot vector are adopted to define boundary elements. For example, the boundary curve of domain Ω is created by the knot vector $\mathcal{E} = \{0001123345566778991010111111\}/11$ and 20 control points as shown in Fig. 1, where the associated basis functions and elements information are illustrated in Fig. 2. In this case, the elements are defined by different knot parameters such as $[0, 1/11]$, $[1/11, 2/11]$, and so on. When the element parameter space is mapped to the physical space, the distribution of collocation points is depicted in Fig. 3. The element connectivity information is shown in Table 1.

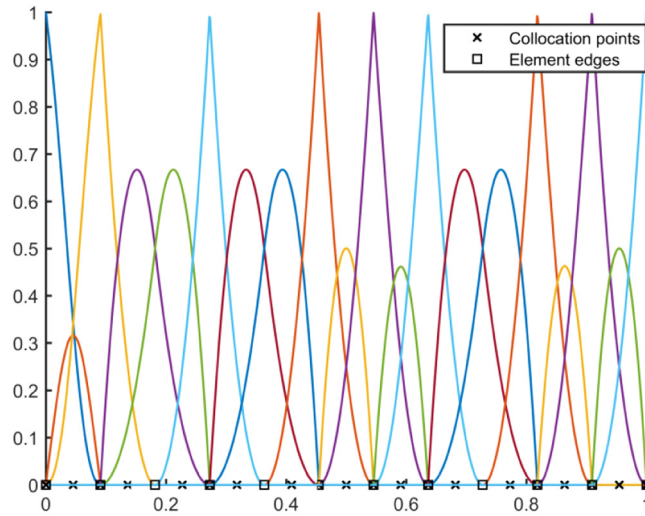


Fig. 2. NURBS basis functions.

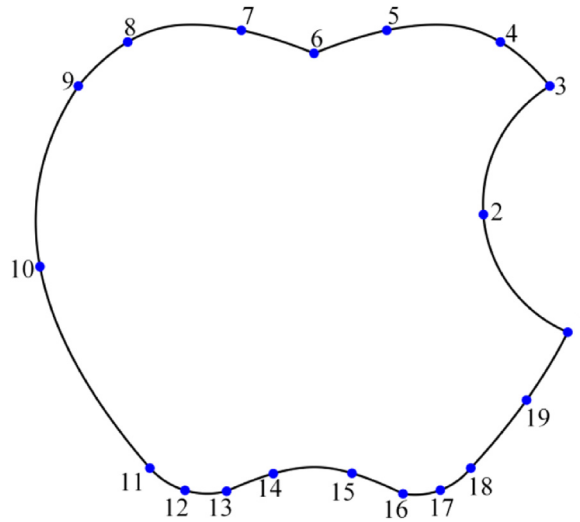


Fig. 3. Distribution of collocation points.

Similar to Eq. (5), the boundary point $\mathbf{x}(\xi)$, the temperature $T(\xi, t)$, the temperature gradient $q(\xi, t)$, the particular solution function $\hat{T}_j(\xi)$ and $\hat{q}_j(\xi)$ are interpolated respectively approximation as

$$\left\{ \begin{aligned} \mathbf{x}(\xi) &= \sum_{a=1}^n R_{a,p}(\xi) \mathbf{x}_a \\ T(\xi, t) &= \sum_{a=1}^n R_{a,p}(\xi) T_a(t) \\ q(\xi, t) &= \sum_{a=1}^n R_{a,p}(\xi) q_a(t) \\ \hat{T}_j(\xi) &= \sum_{a=1}^n R_{a,p}(\xi) \hat{T}_{aj} \\ \hat{q}_j(\xi) &= \sum_{a=1}^n R_{a,p}(\xi) \hat{q}_{aj} \end{aligned} \right. \quad (18)$$

where \mathbf{x}_a , $T_a(t)$, $q_a(t)$, \hat{T}_{aj} and \hat{q}_{aj} are the so-called control variables. Since the basis functions $R_{a,p}$ have a local support, $R_{a,p}(\xi) = 0$ if $\xi \notin [\xi_a, \xi_{a+p+1})$. Based on this, Eq. (18) can be rewritten on each element e as

$$\left\{ \begin{aligned} \mathbf{x}(\xi) &= \sum_{l=1}^{p+1} R_{l,p}^e(\xi) \mathbf{x}_l^e \\ T(\xi, t) &= \sum_{l=1}^{p+1} R_{l,p}^e(\xi) T_l^e(t) \\ q(\xi, t) &= \sum_{l=1}^{p+1} R_{l,p}^e(\xi) q_l^e(t) \\ \hat{T}_j(\xi) &= \sum_{l=1}^{p+1} R_{l,p}^e(\xi) \hat{T}_{lj}^e \\ \hat{q}_j(\xi) &= \sum_{l=1}^{p+1} R_{l,p}^e(\xi) \hat{q}_{lj}^e \end{aligned} \right. \tag{19}$$

For the boundary collocation point $\mathbf{x}_b = \mathbf{x}(\xi_b)$, and Eq. (17) takes the following form:

$$\begin{aligned} & C(\mathbf{x}_b) \sum_{l=1}^{p+1} R_{l,p}^{e'}(\xi_b) T_l^{e'}(t) + \sum_{e=1}^{N_e} \sum_{l=1}^{p+1} \left[\int_{-1}^1 q^*(\mathbf{x}(\xi_b), \mathbf{x}(\hat{\xi})) R_{l,p}^e(\hat{\xi}) J^e(\hat{\xi}) d\hat{\xi} \right] T_l^e(t) \\ & - \sum_{e=1}^{N_e} \sum_{l=1}^{p+1} \left[\int_{-1}^1 T^*(\mathbf{x}(\xi_b), \mathbf{x}(\hat{\xi})) R_{l,p}^e(\hat{\xi}) J^e(\hat{\xi}) d\hat{\xi} \right] q_l^e(t) \\ & = \sum_{j=1}^{N_t} \alpha_j(t) \left\{ C(\mathbf{x}_b) \sum_{l=1}^{p+1} R_{l,p}^{e'}(\xi_b) \hat{T}_{lj}^{e'} + \sum_{e=1}^{N_e} \sum_{l=1}^{p+1} \left[\int_{-1}^1 q^*(\mathbf{x}(\xi_b), \mathbf{x}(\hat{\xi})) R_{l,p}^e(\hat{\xi}) J^e(\hat{\xi}) d\hat{\xi} \right] \hat{T}_{lj}^e \right. \\ & \left. - \sum_{e=1}^{N_e} \sum_{l=1}^{p+1} \left[\int_{-1}^1 T^*(\mathbf{x}(\xi_b), \mathbf{x}(\hat{\xi})) R_{l,p}^e(\hat{\xi}) J^e(\hat{\xi}) d\hat{\xi} \right] \hat{q}_{lj}^e \right\} \end{aligned} \tag{20}$$

where N_e is the number of elements, ξ_b denotes the local coordinate of the collocation point \mathbf{x}_b , e' is the element containing \mathbf{x}_b , the local coordinate system $\hat{\xi} \in [-1, 1]$ is used and the Jacobian of transformation, $J^e(\hat{\xi})$, is given by [19]

$$J^e(\hat{\xi}) = \frac{d\Gamma}{d\xi} \frac{d\xi}{d\hat{\xi}} = \sqrt{\left(\frac{dx_1}{d\xi}\right)^2 + \left(\frac{dx_2}{d\xi}\right)^2} \cdot \frac{\xi_2 - \xi_1}{2} \tag{21}$$

in which ξ_1 and ξ_2 represent the endpoints of the element e in the parameter space. For solving Eq. (20), three different types of integrals are involved, such as regular integration, nearly singular integration and singular integration. In this study, the regular integral is treated in the same way as the nearly singular integral. For the strongly singular integration, we adopt the singularity subtraction technique to solve. For the weakly singular integral, an efficient transformation technique is used to remove the singularity. The detailed integration schemes are introduced in [19].

In order to ensure that the positions of collocation points is on the real boundary in IGBEM, we use the Greville abscissae method [19] to generate the collocation points in parameter space. For example, the i th point is defined by

$$\xi_i' = \frac{\xi_{i+1} + \xi_{i+2} + \dots + \xi_{i+p}}{p} \quad i = 1, 2, \dots, n \tag{22}$$

Using the first formula in Eq. (19), the corresponding collocation point position of ξ_i' in Eq. (22) can be obtained.

Note, the Greville abscissae generates n collocation points, and when Eq. (20) is prescribed at each collocation point, it yields a system of n equations. The definition of functions \hat{T}_j and \hat{q}_j in Eqs. (14)–(15) involves N_t points \mathbf{x}_j , which need to be defined. We assume, that N_t includes N_b points on the boundary and N_i points inside the domain, i.e. $N_t = N_b + N_i$. We consider that the boundary points \mathbf{x}_j coincide with the collocation points \mathbf{x}_b defined by the Greville abscissae and therefore $N_b = n$. The set of N_i points \mathbf{x}_j inside the domain will be also used to collocate Eq. (17) and will be denoted by

\mathbf{x}_i . At these points $C(\mathbf{x}_i) = 1$ and the discretized integral equation (17) takes the form

$$\begin{aligned}
 & T(\mathbf{x}_i, t) + \sum_{e=1}^{N_e} \sum_{l=1}^{p+1} \left[\int_{-1}^1 q^* (\mathbf{x}_i, \mathbf{x}(\hat{\xi})) R_{l,p}^e(\hat{\xi}) J^e(\hat{\xi}) d\hat{\xi} \right] T_l^e(t) \\
 & - \sum_{e=1}^{N_e} \sum_{l=1}^{p+1} \left[\int_{-1}^1 T^* (\mathbf{x}_i, \mathbf{x}(\hat{\xi})) R_{l,p}^e(\hat{\xi}) J^e(\hat{\xi}) d\hat{\xi} \right] q_l^e(t) \\
 & = \sum_{j=1}^{N_t} \alpha_j(t) \left\{ \hat{T}_j(\mathbf{x}_i) + \sum_{e=1}^{N_e} \sum_{l=1}^{p+1} \left[\int_{-1}^1 q^* (\mathbf{x}_i, \mathbf{x}(\hat{\xi})) R_{l,p}^e(\hat{\xi}) J^e(\hat{\xi}) d\hat{\xi} \right] \hat{T}_{lj}^e \right. \\
 & \left. - \sum_{e=1}^{N_e} \sum_{l=1}^{p+1} \left[\int_{-1}^1 T^* (\mathbf{x}_i, \mathbf{x}(\hat{\xi})) R_{l,p}^e(\hat{\xi}) J^e(\hat{\xi}) d\hat{\xi} \right] \hat{q}_{lj}^e \right\}
 \end{aligned} \tag{23}$$

where values of temperature at internal points $T(\mathbf{x}_i, t)$ form a new set of N_i unknowns. As a result, coupled Eqs. (20) and (23) yield the full system of N_t equations for N_t unknowns, which can be written in the matrix form as

$$\mathbf{HT}(t) - \mathbf{Gq}(t) = \sum_{j=1}^{N_t} \alpha_j(t) (\mathbf{HT}_j - \mathbf{Gq}_j) \tag{24}$$

where the vector $\mathbf{T}(t) = \mathbf{T}$ ($\mathbf{T} \in \mathbb{R}^{N_t \times 1}$) is expressed as

$$\mathbf{T} = [T_1, T_2, \dots, T_{N_b}, T_{N_b+1}, T_{N_b+2}, \dots, T_{N_t}]^T \tag{25}$$

The first N_b elements in the vector \mathbf{T} represent the temperature coefficients of control points (i.e. control variables $T_i(t)$ in Eq. (18)). The last N_i elements denote the temperature of the internal nodes, i.e.

$$T_i = T(\mathbf{x}_i, t), \quad i = N_b + 1, \dots, N_t \tag{26}$$

The vector $\mathbf{q}(t) = \mathbf{q}$ ($\mathbf{q} \in \mathbb{R}^{N_b \times 1}$) contains temperature gradients of the control points in Eq. (18) and can be expressed as

$$\mathbf{q} = [q_1, q_2, \dots, q_{N_b}]^T \tag{27}$$

The vectors $\hat{\mathbf{T}}_j$ ($\hat{\mathbf{T}}_j \in \mathbb{R}^{N_t \times 1}$) in Eq. (24) can be written as

$$\hat{\mathbf{T}}_j = [\hat{T}_{1j}, \hat{T}_{2j}, \dots, \hat{T}_{N_bj}, \hat{T}_{(N_b+1)j}, \dots, \hat{T}_{N_tj}]^T, \quad \hat{T}_{lj} = \hat{T}_j(\mathbf{x}_l), \quad l = 1, 2, \dots, N_t \tag{28}$$

where $\{\mathbf{x}_l\}_{l=1}^{N_t}$ denotes the full set of collocation points. The vectors $\hat{\mathbf{q}}_j$ ($\hat{\mathbf{q}}_j \in \mathbb{R}^{N_b \times 1}$) are written as

$$\hat{\mathbf{q}}_j = [\hat{q}_{1j}, \hat{q}_{2j}, \dots, \hat{q}_{N_bj}]^T, \quad \hat{q}_{lj} = \hat{q}_j(\mathbf{x}_l), \quad l = 1, 2, \dots, N_b \tag{29}$$

Next, we introduce matrices $\hat{\mathbf{T}}$ ($\hat{\mathbf{T}} \in \mathbb{R}^{N_t \times N_t}$), $\hat{\mathbf{q}}$ ($\hat{\mathbf{q}} \in \mathbb{R}^{N_t \times N_b}$) consisting of vectors $\hat{\mathbf{T}}_j$ and $\hat{\mathbf{q}}_j$ (as columns), and time-dependent vector $\boldsymbol{\alpha} = \boldsymbol{\alpha}(t)$ ($\boldsymbol{\alpha} \in \mathbb{R}^{N_t \times 1}$) which is used to write the inversion of Eq. (12), evaluated at N_t collocation points, i.e.

$$\boldsymbol{\alpha} = \mathbf{F}^{-1} \mathbf{b} \tag{30}$$

where $\mathbf{F} \in \mathbb{R}^{N_t \times N_t}$, $\mathbf{b} = \mathbf{b}(t) \in \mathbb{R}^{N_t \times 1}$. Components of matrix \mathbf{F} are defined by

$$F_{lj} = f_j(\mathbf{x}_l) \tag{31}$$

where function f_j are given by Eq. (13). Vector \mathbf{b} represents the right hand side of Eq. (11), i.e. its components contain unknown time derivatives $\partial T(\mathbf{x}_l, t)/\partial t$ evaluated at collocation points \mathbf{x}_l :

$$b_l = \frac{1}{\lambda} \frac{\partial T(\mathbf{x}_l, t)}{\partial t} - \frac{1}{k} g(\mathbf{x}_l, t) \tag{32}$$

Finally, Eq. (24) is given as

$$\mathbf{HT}(t) = \mathbf{Gq}(t) - \mathbf{Sb}(t) \tag{33}$$

where

$$\mathbf{S} = -(\mathbf{HT} - \mathbf{Gq}) \mathbf{F}^{-1} \tag{34}$$

Eq. (33) contains three time-dependent unknowns, namely vectors $\mathbf{T}(t)$, $\mathbf{q}(t)$ and $\mathbf{b}(t)$, which will be approximated using two-level time integration scheme [45].

4.3. Two-level time integration scheme

In what follows, we will use the following notations: Δt is the time step, m th time interval is denoted as $[t_m, t_{m+1}]$, all quantities evaluated at time t_m will be denoted with superscript m . According to the two-level time integration scheme, on a time interval $[t_m, t_{m+1}]$, each component of vectors $\mathbf{T}(t)$, $\mathbf{q}(t)$ and the heat source $g(t)$ are approximated as a linear combination of the corresponding values at the end-points t_m and t_{m+1} and three parameters, θ_T , θ_q and θ_g , as

$$\begin{cases} T_l(t) = (1 - \theta_T) T_l^m + \theta_T T_l^{m+1} \\ q_l(t) = (1 - \theta_q) q_l^m + \theta_q q_l^{m+1} \\ g_l(t) = (1 - \theta_g) g_l^m + \theta_g g_l^{m+1} \\ \frac{\partial T_l(t)}{\partial t} = \frac{T_l^{m+1} - T_l^m}{\Delta t} \end{cases} \tag{35}$$

Based on this approximation, the first N_b elements in the vector \mathbf{b} can be expressed in the temperature coefficients of the control points as

$$b_l(t) = \frac{1}{\lambda \Delta t} \sum_{i=1}^{N_b} R_{i,p}(\xi_i) (T_i^{m+1} - T_i^m) - \left[(1 - \theta_g) \frac{g_l^m}{k} + \theta_g \frac{g_l^{m+1}}{k} \right], (l = 1, 2, \dots, N_b) \tag{36}$$

where points ξ_l correspond to the parametric coordinates of the boundary collocation points \mathbf{x}_l . The last N_i elements are expressed in terms of the temperature value at the internal nodes, i.e.

$$b_l = \frac{1}{\lambda \Delta t} (T_l^{m+1} - T_l^m) - \left[(1 - \theta_g) \frac{g_l^m}{k} + \theta_g \frac{g_l^{m+1}}{k} \right], (l = N_b + 1, N_b + 2, \dots, N_t) \tag{37}$$

Combining Eq. (36) with (37), the vector \mathbf{b} can be written as

$$\mathbf{b} = \frac{1}{\lambda \Delta t} \mathbf{R} (\mathbf{T}^{m+1} - \mathbf{T}^m) - \frac{1}{k} [(1 - \theta_g) \mathbf{g}^m + \theta_g \mathbf{g}^{m+1}] \tag{38}$$

where matrix $\mathbf{R} \in \mathbb{R}^{N_t \times N_t}$ is given by

$$\mathbf{R} = \begin{bmatrix} (\mathbf{R}_\Delta)_{N_b \times N_b} & \mathbf{0} \\ \mathbf{0} & \mathbf{I}_{N_i \times N_i} \end{bmatrix} \tag{39}$$

in which components of \mathbf{R}_Δ are $R_{\Delta \ l m} = R_{l,p}(\xi_m)$ and components of vector \mathbf{g}^i are $g_l^i = g(\mathbf{x}_l, t_i)$, $i = m$ or $m + 1$.

Substituting Eqs. (35) and (38) into Eq. (33) yields

$$\begin{aligned} \left(\frac{1}{\lambda \Delta t} \mathbf{S} \mathbf{R} + \theta_T \mathbf{H} \right) \mathbf{T}^{m+1} - \theta_q \mathbf{G} \mathbf{q}^{m+1} &= \left[\frac{1}{\lambda \Delta t} \mathbf{S} \mathbf{R} - (1 - \theta_T) \mathbf{H} \right] \mathbf{T}^m \\ &+ (1 - \theta_q) \mathbf{G} \mathbf{q}^m + \frac{\mathbf{S}}{k} [(1 - \theta_g) \mathbf{g}^m + \theta_g \mathbf{g}^{m+1}] \end{aligned} \tag{40}$$

The right side of Eq. (40) is known at any time t_m , since it involves quantities which have been specified as the initial conditions, known heat source or calculated at previous time steps. Note, that some of the terms in vectors \mathbf{T}^{m+1} and \mathbf{q}^{m+1} are known from the boundary conditions, and the remaining unknown terms can be evaluated at each time t_{m+1} . Note that the elements of matrices \mathbf{S} , \mathbf{R} , \mathbf{H} and \mathbf{G} depend only on the geometrical data. Therefore, they can all be computed once and stored. For the heat source vector \mathbf{g} , it can be also computed once when \mathbf{g} is time-independent. The detailed flow chart of the method is shown in Fig. 4.

After the above calculation process, the solutions of all control points and selected interior points are obtained. The temperature values of any points in domain can be obtained by using Eq. (23), and the solution of interior point of element on the boundary can be obtained by substituting the parameter corresponding to that point into Eq. (19).

5. Numerical examples

In this section, several different geometries with different boundary conditions are discussed. In all examples in this chapter it is assumed that $k = 1$, $c = 1$, $\rho = 1$. where the thermal conductivity, the density and the specific heat are assumed as unit. It is worth noting that in order to start the calculation process automatically, the parameters θ_T , θ_q and θ_g in Eq. (40) take value 1 at the first time step and the rest of time steps are taken as 0.5. To show the case of overall errors, the relative L_2 error norm in temperatures is calculated by

$$e_{L_2} = \frac{\|\mathbf{T}_{num} - \mathbf{T}_{exact}\|_{L_2}}{\|\mathbf{T}_{exact}\|_{L_2}} \tag{41}$$

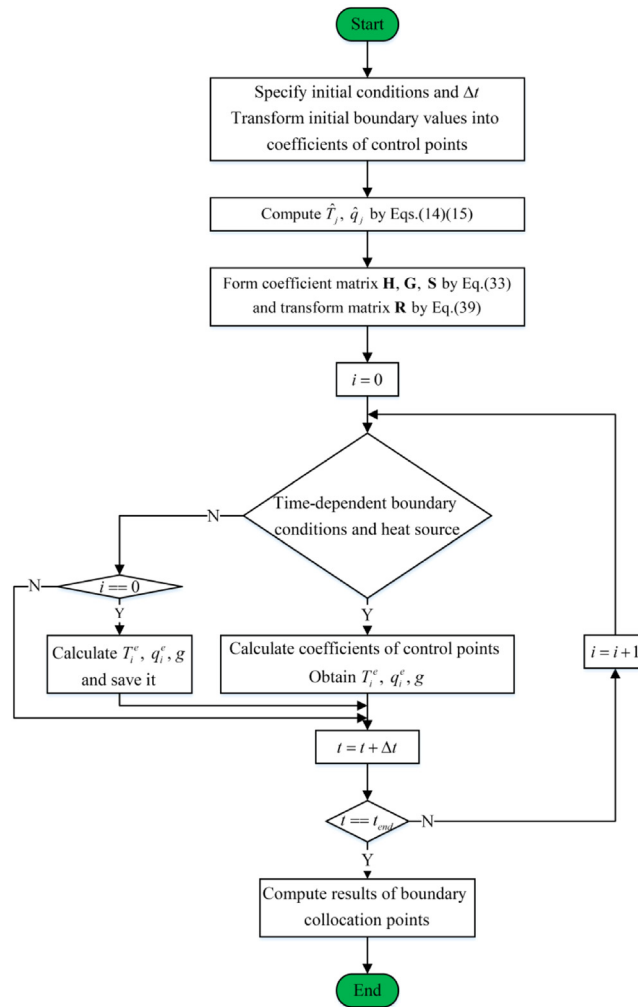


Fig. 4. Flow chart of IG-DRBEM.

where

$$\|\mathbf{T}_{\text{exact}}\|_{L_2} = \sqrt{\sum_{i=1}^{N_t} T_i^2} \tag{42}$$

5.1. An infinite slab subject to a thermal shock

An infinite slab, which is the same as example 1 in [48], is considered here to compare the IG-DRBEM with the conventional DRBEM, and the effect of different time steps on the result is discussed here. The problem is modeled as a two-dimensional with mixed boundary conditions, namely $T = 1$ prescribed along the faces $x = \pm 5$ and $q = 0$ along the faces $y = \pm 4$ of a rectangular region. The initial temperature is specified as $T_0 = 0$. Results are presented for the temperature at the center point $(0, 0)$. Because of the symmetry of the problem, a quarter of the region is computed as the same in [48]. In this example, all the results are obtained by one-order expansion function ($f_j = 1 + r_j$), two-order elements and one interior point. In order to improve the accuracy of results, we refer to the distribution method of element in literature [48]. Because this term $\partial T / \partial t$ always equals to zero when $t > 0$. A small number of elements are applied on the boundary of thermal shock and a relatively large number of elements are distributed on other boundaries.

Here, two cases of different element numbers are computed. The information of control points of 7 and 14 IGA elements is shown in Fig. 5(a) and (b). Both traditional DRBEM and IG-DRBEM use an interior point and the same node freedom degree. It can be seen from Tables 2 and 3 that IG-DRBEM obtains more accurate results than DRBEM, and even IG-DRBEM applies less 7 elements as shown in Table 2.

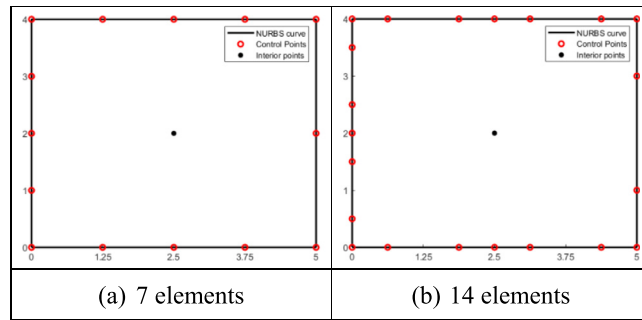


Fig. 5. Control points and interior points for different number of elements.

Table 2
Temperature and absolute errors (Abserr) at the point (0, 0) of 7 elements.

Time	Exact [68]	DRBEM [48]	Abserr	IG-DRBEM	Abserr
2	0.025	0.017	0.008	0.025	0
4	0.154	0.166	0.012	0.151	0.003
6	0.298	0.302	0.004	0.298	0
8	0.422	0.418	0.004	0.424	0.002
10	0.526	0.516	0.010	0.528	0.002
15	0.710	0.694	0.016	0.715	0.005
20	0.823	0.807	0.016	0.827	0.004
30	0.934	0.923	0.011	0.937	0.003

Table 3
Temperature and Abserr at the point (0, 0) of 14 elements.

Time	Exact [68]	DRBEM [48]	Abserr	IG-DRBEM	Abserr
2	0.025	0.017	0.008	0.026	0.001
4	0.154	0.166	0.012	0.152	0.002
6	0.298	0.302	0.004	0.298	0
8	0.422	0.418	0.004	0.424	0.002
10	0.526	0.516	0.010	0.529	0.003
15	0.710	0.694	0.016	0.715	0.005
20	0.823	0.807	0.016	0.827	0.004
30	0.934	0.923	0.011	0.937	0.003

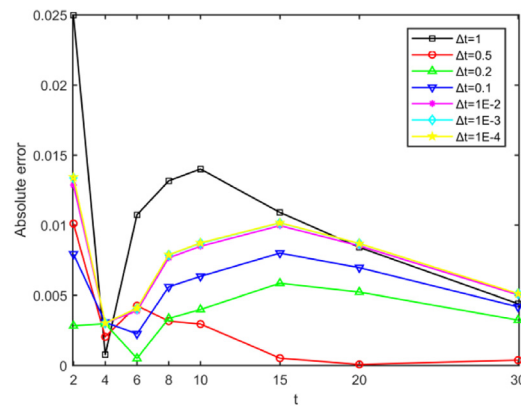


Fig. 6. Results using different time steps.

To investigate the effect of time steps on numerical results, the results of point (0, 0) based on the element distribution in Fig. 5(a) are shown in Fig. 6. It can be seen that the absolute error fluctuates greatly in the initial stage, and the time step has a certain influence on the numerical results. With the increase of computation time, the influence of time step on the results also tends to be stable. Of course, the time step should not be too small to avoid the cumulative error. Therefore, in the calculation process, the appropriate time step size can be selected according to different element distributions.

Table 4
Temperature and relative errors of the point (0, 0) using different interior points at $t = 0.5$.

N_i	IG-DRBEM	Exact	Relative error (%)
1	1.6379		0.66
13	1.6487		0.0
25	1.6491	1.6487	0.024
37	1.6494		0.042
49	1.6495		0.049
109	1.6496		0.055

Table 5
Results for different expansions of f_j .

f_j	Mabserr	Mrelerr (%)	e_{L_2}
(i)	0.002496	0.09182	3.2371e-04
(ii)	0.002520	0.1529	5.3262e-04
(iii)	0.002208	0.1623	5.3053e-04

5.2. A circular plate

In this example, a circular plate with the temperature boundary condition is considered without heat sources to test the effect of the number of interior points and the expansion order and verify the validity and convergence of the presented method. The initial condition and the exact solution are given by $T_0 = e^x$ and $T = e^{x+t}$, respectively. The time step is taken as 0.01 and the temperature results at $t = 0.5$ are shown in following cases.

(A) The influence of the number of interior points

First of all, we consider the influence of the number of interior points on the results. Six sets of interior points are used as shown in Fig. 7, where the circular boundary is discretized as eight two-order elements with 13 control points. In this case, the one-order expansion function $f_j = 1 + r_j$ is used.

To show the effect of different interior points on the results, the relative errors are shown in Table 4, where the relative error can be expressed as $100 \cdot |T_{exact} - T_{exact}| / |T_{exact}|$. It can be seen from Table 4 that the sensitivity of the results to the number of interior points is small. The total variation of results from $N_i = 1$ to $N_i = 109$ is no more than 0.7%. This conclusion is similar to page 94 of the book [47]. Especially, the results tend to be more stable when the interior point are more than 25. For IG-DRBEM, a few interior points are distributed in the domain to ensure that the whole domain can be described accurately when the domain integral is transformed. Too few interior points cannot accurately describe the change of the field, and too many interior points will cause the ill-condition of the transformation matrix of the domain integral matrix to some extent. Therefore, we only need a few interior points when using IG-DRBEM. If we need to calculate the temperature at any position in the domain, we can calculate with the obtained boundary control points and the values of the points in the domain.

(B) The influence of different expressions of f

In this case, the three forms of expansion are considered as follows

- (i) $f_j = 1 + r_j$
- (ii) $f_j = 1 + r_j + r_j^2$
- (iii) $f_j = 1 + r_j + r_j^2 + r_j^3$

The information of the element division and the distribution of internal points in Fig. 7(b) are adopted to test the effect of the different order expansions on the results.

It can be seen from Table 5 that the maximum absolute error (Mabserr) and the maximum relative error (Mrelerr) are no more than 0.0026 and 0.17%, respectively. Obviously, the best result is obtained by using case (i), which used the simplest expansion $f_j = 1 + r_j$. Similar to the conclusion for the page 115 of the book [47], these results indicate that the higher-order f_j expansions are unnecessary. Based on this, the expansion $f_j = 1 + r_j$ is adopted in the following examples.

5.3. A quarter annulus

To show the convergence and the ability to compute the temperature of arbitrary interior point on the boundary element, a quarter annulus is considered without heat sources. Similar to Section 5.2, the exact solution still can be given by $T = e^{x+t}$. The geometry and boundary conditions are shown in Fig. 8, and the initial condition is given by $T_0 = e^x$. The h -refinement [12] is used to form the uniform refinement applied around the boundary for both $p = 2$ and $p = 3$, where 9 interior points are used as shown in Fig. 9. In this case, to test the convergence of the present method, the results at $t = 1$ are presented in Fig. 10. In this example, the time step $\Delta t = 0.001$ is used. It can be seen from Fig. 10 that the e_{L_2} of results become smaller and smaller with the increase of elements. Also, compared with the result of $p = 2$, the result

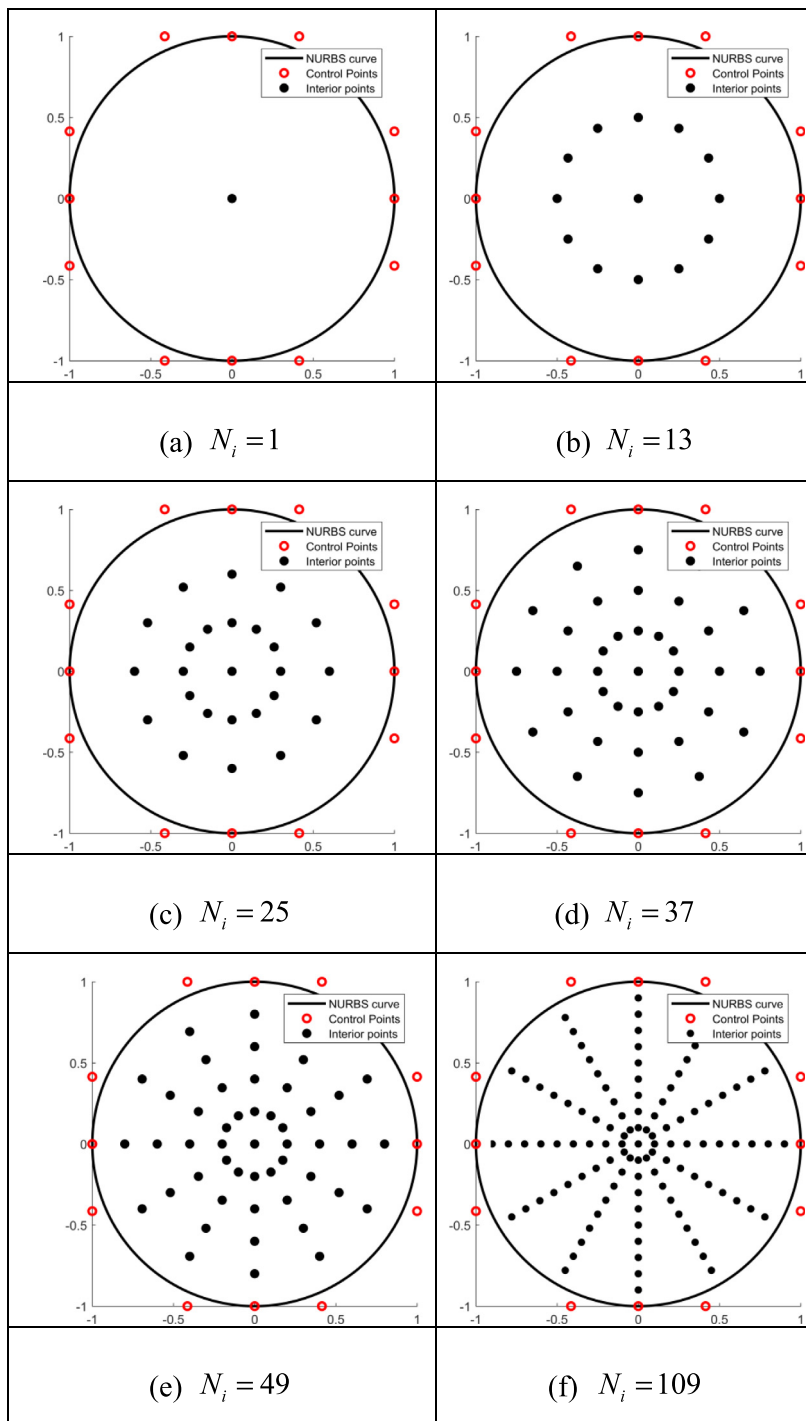


Fig. 7. Different numbers of interior points.

of $p = 3$ converges faster. It is worth noting that even if the most sparse element distribution is used at $p = 2$, the e_{l_2} can also reach to 10^{-2} magnitude.

After obtaining the unknown quantities of boundary control points and distribution points in the inner domain, the results of some randomly selected interior points can be computed by the obtained corresponding quantities. As shown in Fig. 9(b), the randomly selected six interior points of element are used to demonstrate the validity by obtained

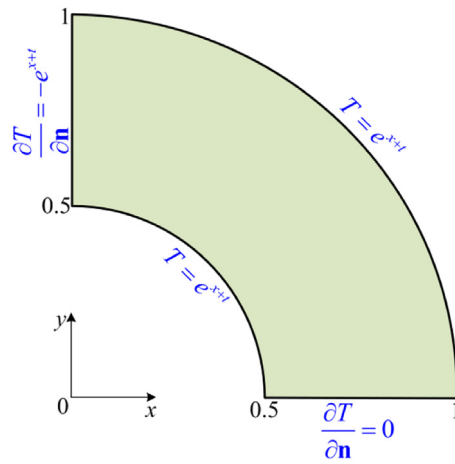


Fig. 8. Geometry and boundary conditions.

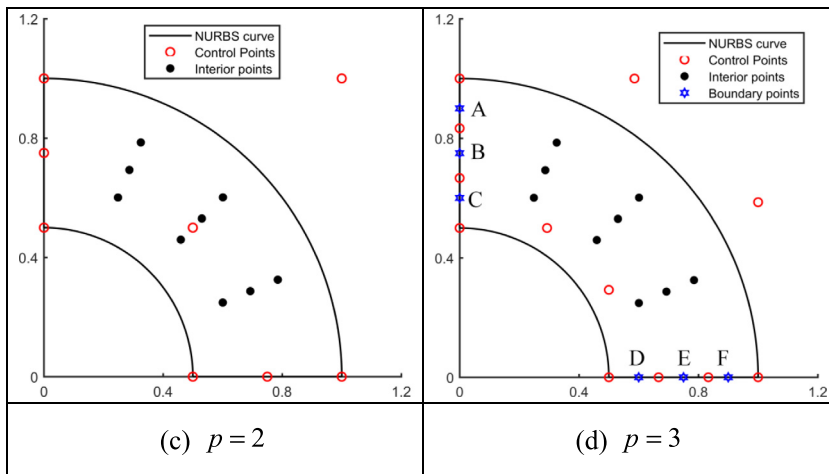


Fig. 9. Isogeometric computation model without element refinement.

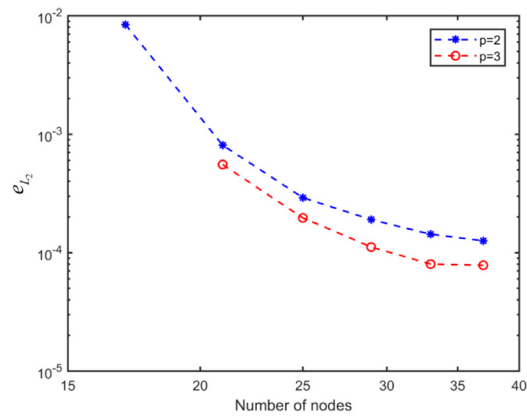


Fig. 10. e_{L_2} of different number of nodes.

temperature of control points and interior points in domain. It can be seen from Fig. 11 that the absolute errors can be achieved 10^{-3} magnitude.

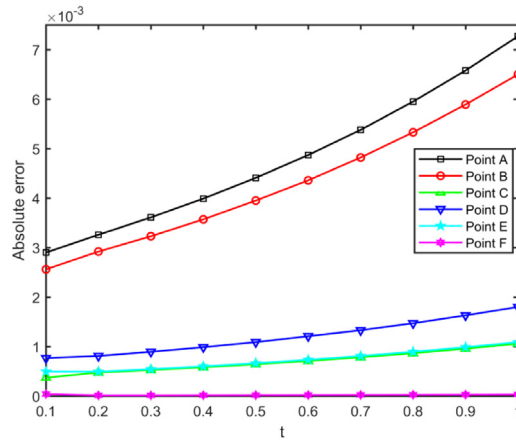


Fig. 11. Absolute errors of results for different points.

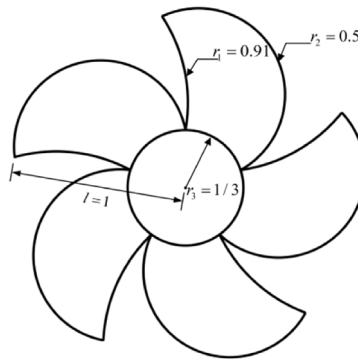


Fig. 12. Geometry description.

Table 6
Computational information of marine propeller model and the error of results on the $t = 1$.

Case	N_e	N_t	e_{L_2}	Mabserr
(a)	19	88	$9.06e-3$	0.021
(b)	38	107	$4.64e-3$	0.017

5.4. Marine propeller

To verify the ability of the proposed method to handle complex engineering geometries, similar to the literature [69], a marine propeller is analyzed with the temperature boundary condition. As shown in Fig. 12, the inner and outer radius of the blade are taken as $r_1 = 0.91$ and $r_2 = 0.5$, respectively. The radius of interior circle is $r_3 = 1/3$. The distance between the center and the blade corners is $l = 1$. The knot vector of outer blades is

$$\begin{aligned} \mathcal{E}_1 = \{ & 0, 0, 0, 1, 1, 2, 2, 3, 3, 4, 4, \\ & 5, 5, 6, 6, 7, 7, 8, 8, 9, 9, 10, \\ & 10, 11, 11, 12, 12, 13, 13, 14, 14, \\ & 15, 15, 15 \} / 15 \end{aligned} \tag{43}$$

and the knot vector of interior circle is

$$\mathcal{E}_2 = \{ 0, 0, 0, 1/4, 1/4, 2/4, 2/4, 3/4, 3/4, 1, 1, 1 \} \tag{44}$$

As shown in Fig. 13, 50 interior points are distributed into the marine propeller. In this case, the initial condition and the heat source are specified as $T_0 = 0$ and $g = 10xy \cos(2t)$, respectively. The exact solution is given by $T = 10xy \sin(t) \cos(t)$. The temperature boundary conditions are imposed by the form of the exact solution in the solving process.

In this example, the time step $\Delta t = 0.01$ is adopted. The two partitions of elements are considered with $p = 2$ as shown in Fig. 13(a) and (b). The detailed calculation information and result errors are shown in Table 6, which the e_{L_2}

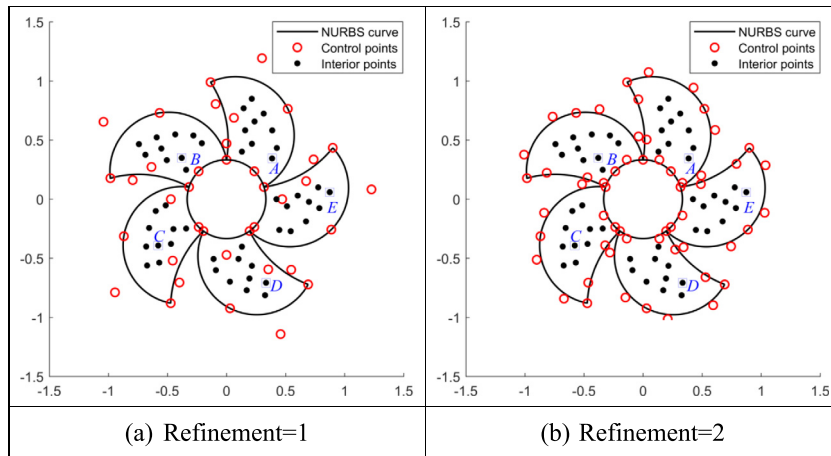


Fig. 13. Marine propeller with $p = 2$.

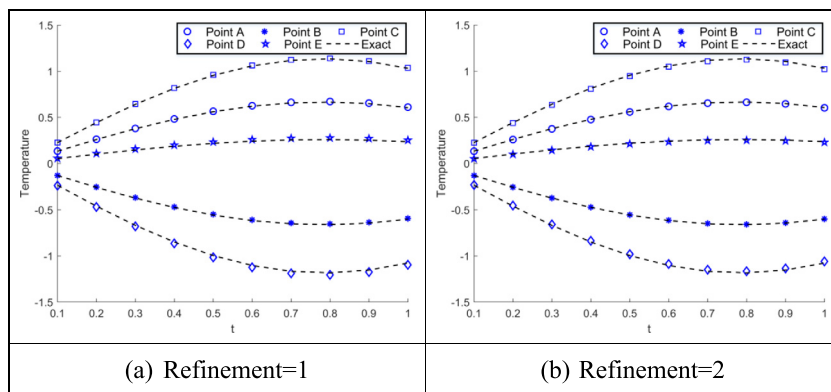


Fig. 14. Temperature of different points on the different time.

reduces when the distribution of element is refined one time such as Fig. 13(b) and the maximum absolute error of all nodes is no more than 0.017. It is worth noting that even in the case of sparse elements such as Fig. 13(a), the error e_{L_2} can still reach to 10^{-3} magnitude. In addition, it can be seen from Fig. 14 that the temperature of five randomly selected points is in good agreement with the analytic solution, even if the relatively sparse element partition is adopted. Therefore, the present method has a good ability to adapt to complex geometric shapes, even when dealing with problems with heat sources.

5.5. Quarter gear

To show the performance of the proposed method to solve the complex geometry with the mixed boundary conditions and heat sources, a quarter gear with a hole is considered as shown in Fig. 15, where the inner radius of the gear is $r_1 = 0.2$, the radius of the addendum circle is $r_4 = 1.4$, the center angle of the annulus is $\varphi = 30^\circ$, the inner radius and the outer radius of the annulus hole are $r_2 = 0.5$ and $r_3 = 0.7$, respectively. The length of the left vertical edge and the bottom horizontal edge is $L_1 = 0.8$. The dedendum width and the addendum width are $L_3 = 0.39$ and $L_4 = 0.195$, respectively.

The initial temperature and the heat source are specified as $T_0 = 0$ and $g = xy$, respectively. The temperature gradient condition $\partial T / \partial \mathbf{n}$ is applied to the left vertical edge and the bottom horizontal boundary, and the rest of the boundary is applied the temperature condition such as $\bar{T} = xyt$. The exact solution is given by $T = xyt$. In this example, the time step $\Delta t = 0.01$ is adopted. As shown in Fig. 16, the two partitions of element with $p = 3$ are used, where the knot vectors of outer and inner boundary are expressed as

$$\mathcal{E}_1 = \{000011223344556677 \\ 8889991010101111\}/11; \tag{45}$$

$$\mathcal{E}_2 = \{00001/41/41/41/21/21/23/43/43/41111\} \tag{46}$$

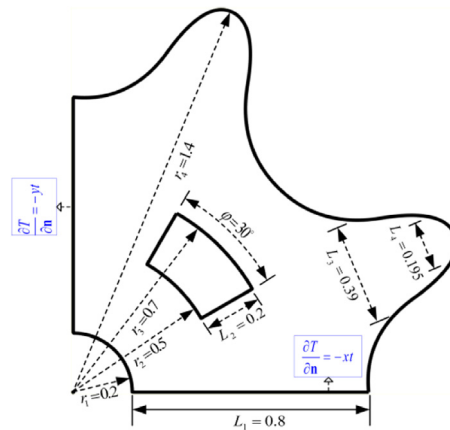


Fig. 15. Geometry description and boundary conditions.

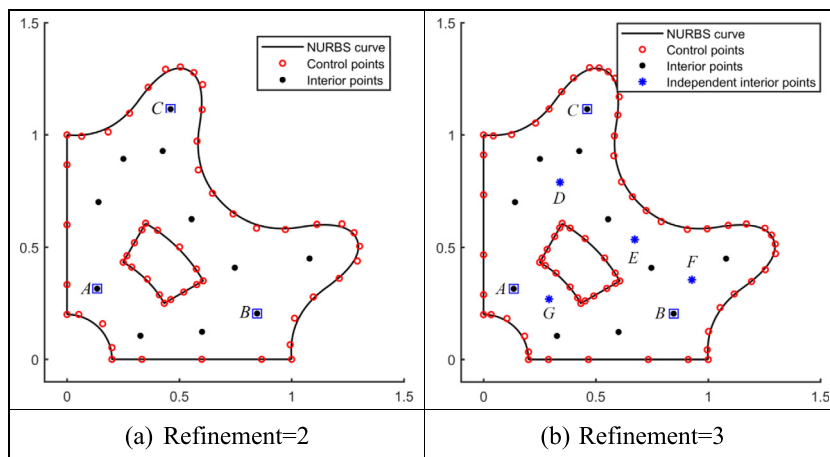


Fig. 16. Quarter gear with $p = 3$.

Table 7
Computational information of gear model and the error of results on the $t = 1$.

Case	N_e	N_t	e_{l_2}	Mabserr
(a)	30	64	$1.01e-2$	$1.24e-2$
(b)	45	79	$8.47e-3$	$9.90e-3$

The detailed calculation information and result errors are shown in Table 7, which the e_{l_2} and the Mabserr are reduced with the refinement of element such as Fig. 16. Also, the Mabserr is no more than $9.90e-3$. It can be seen from Fig. 17 that the temperature results of the three interior points of the randomly selected $A(0.1342, 0.3152)$, $B(0.8463, 0.2043)$, $C(0.4611, 1.1148)$ are in good agreement with the exact solutions, even in the case of sparse elements. Therefore, the proposed method can obtain better numerical results with mixed boundary conditions and heat sources for complex geometries.

A certain number of interior points are selected in our calculation process to improve the accuracy of the overall calculation. If the user wants to obtain the temperature field of any point in the domain, similar to the traditional DRBEM, the obtained values of boundary control points and the points in the domain can be used for calculation. As shown in Fig. 16(b), after calculating unknown quantities of control points and the points in the domain, we calculated the temperature of newly added points in the domain such as $D(0.3404, 0.7893)$, $E(0.6733, 0.5349)$, $F(0.9277, 0.3554)$, $G(0.2918, 0.2693)$, as shown in Fig. 18. It can be seen that the Mabserr also is no more than $9.0e-3$. Therefore, IG-DRBEM inherits the function of the traditional BEM to solve any interior point in the domain by using the obtained boundary and interior quantity information without reducing the precision.

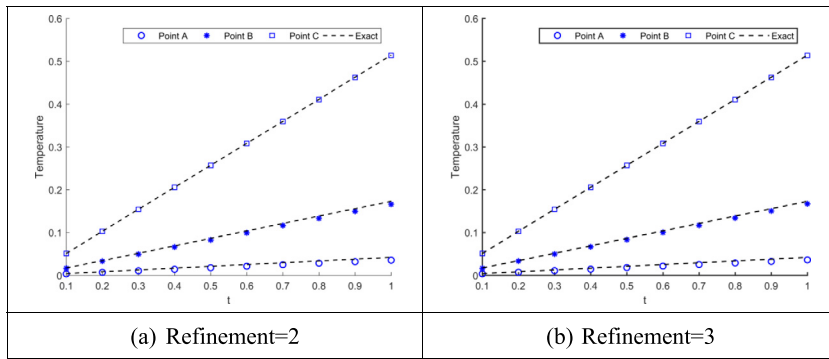


Fig. 17. Temperature of different points on the different time.

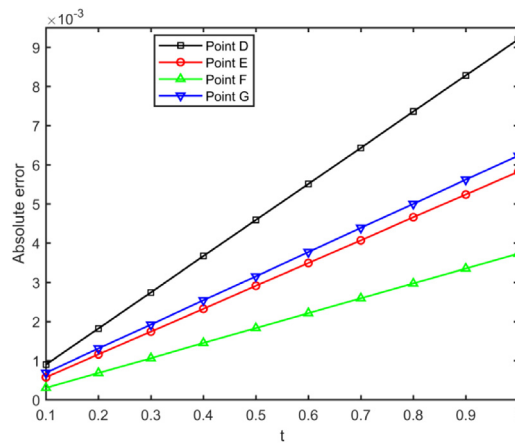


Fig. 18. Absolute errors of results for independent interior points.

6. Conclusions

In this paper, the isogeometric boundary element method is realized for the first time to solve the transient heat transfer problem with heat sources. As a classical and effective domain integral transformation method, the dual reciprocity method makes it possible to analyze complex problems by isogeometric boundary element method, and does not need to divide elements in domain, such as heterogeneous problems, complex dynamic problems and so on. Because even if the fundamental solutions of these problems cannot be obtained, we can still use the fundamental solutions of the approximate problems to establish the integral equations, and the domain integral will be transformed by the dual reciprocity method. Several typical examples show the effectiveness of the presented method and the convenience of dealing with complex geometric problems. The temperature of boundary points excluding control points can be computed by NURBS interpolation using the corresponding element information. In addition, IG-DRBEM inherits the function of the traditional BEM to solve any interior point in the domain by using the obtained boundary and interior quantity information without reducing the precision. The proposal of isogeometric dual reciprocity BEM will provide a new idea for the analysis of transient, heterogeneous and even nonlinear problems, and will promote the development of isogeometric BEM to some extent.

Acknowledgments

The research was supported by the National Natural Science Foundation of China (No. 11872166), the International Postdoctoral Exchange Fellowship Program of China (No. 20180096) and China Postdoctoral Science Foundation (No. 2016M592042).

References

- [1] G.E. Blandford, A.R. Ingraffea, J.A. Liggett, Two-dimensional stress intensity factor computations using the boundary element method, *Int. J. Numer. Methods Engrg.* 17 (3) (1981) 387–404.
- [2] S.T. Grilli, J. Skourup, I.A. Svendsen, An efficient boundary element method for nonlinear water waves, *Eng. Anal. Bound. Elem.* 6 (2) (1989) 97–107.
- [3] S. Kagami, I. Fukai, Application of boundary-element method to electromagnetic field problems (short papers), *IEEE Trans. Microw. Theory Techn.* 32 (4) (1984) 455–461.
- [4] D.L. Karabalis, D.E. Beskos, Dynamic response of 3-D rigid surface foundations by time domain boundary element method, *Earthquake Eng. Struct. Dyn.* 12 (1) (1984) 73–93.
- [5] L.C. Wrobel, *The Boundary Element Method, Applications in Thermo-Fluids and Acoustics*, John Wiley & Sons, 2002.
- [6] R. Bharadwaj, A. Windemuth, S. Sridharan, B. Honig, A. Nicholls, The fast multipole boundary element method for molecular electrostatics: An optimal approach for large systems, *J. Comput. Chem.* 16 (7) (1995) 898–913.
- [7] Y. Liu, *Fast Multipole Boundary Element Method: Theory and Applications in Engineering*, Cambridge university press, 2009.
- [8] N. Nishimura, K.I. Yoshida, S. Kobayashi, A fast multipole boundary integral equation method for crack problems in 3D, *Eng. Anal. Bound. Elem.* 23 (1) (1999) 97–105.
- [9] Y.J. Liu, N. Nishimura, The fast multipole boundary element method for potential problems: a tutorial, *Eng. Anal. Bound. Elem.* 30 (5) (2006) 371–381.
- [10] L. Shen, Y.J. Liu, An adaptive fast multipole boundary element method for three-dimensional acoustic wave problems based on the Burton–Miller formulation, *Comput. Mech.* 40 (3) (2007) 461–472.
- [11] Y.J. Liu, N. Nishimura, Y. Otani, Large-scale modeling of carbon-nanotube composites by a fast multipole boundary element method, *Comput. Mater. Sci.* 34 (2) (2005) 173–187.
- [12] S. Kurz, O. Rain, S. Rjasanow, The adaptive cross-approximation technique for the 3D boundary-element method, *IEEE Trans. Magn.* 38 (2) (2002) 421–424.
- [13] T.J.R. Hughes, J.A. Cottrell, Y. Bazilevs, Isogeometric analysis: CAD, finite elements, nurbs, exact geometry and mesh refinement, *Comput. Methods Appl. Mech. Engrg.* 194 (39–41) (2005) 4135–4195.
- [14] F. Auricchio, L.B. Da Veiga, T.J.R. Hughes, A. Reali, G. Sangalli, Isogeometric collocation methods, *Math. Models Methods Appl. Sci.* 20 (11) (2010) 2075–2107.
- [15] M.R. Moosavi, A. Khelil, Isogeometric meshless finite volume method in nonlinear elasticity, *Acta Mech.* 226 (1) (2015) 123–135.
- [16] S. Natarajan, J. Wang, C. Song, C. Birk, Isogeometric analysis enhanced by the scaled boundary finite element method, *Comput. Methods Appl. Mech. Engrg.* 283 (2015) 733–762.
- [17] P. Li, J. Liu, G. Lin, P.C. Zhang, G.T. Yang, A NURBS-based scaled boundary finite element method for the analysis of heat conduction problems with heat fluxes and temperatures on side-faces, *Int. J. Heat Mass Transfer* 133 (2017) 764–779.
- [18] G. Lin, P. Li, J. Liu, P.C. Zhang, Transient heat conduction analysis using the NURBS-enhanced scaled boundary finite element method and modified precise integration method, *Acta Mech. Solida Sin.* 30 (5) (2017) 445–464.
- [19] R.N. Simpson, S.P.A. Bordas, J. Trevelyan, T. Rabczuk, A two-dimensional isogeometric boundary element method for elastostatic analysis, *Comput. Methods Appl. Mech. Engrg.* 209 (2012) 87–100.
- [20] M.A. Scott, R.N. Simpson, J.A. Evans, S. Lipton, S.P.A. Bordas, T.J.R. Hughes, T.W. Sederberg, Isogeometric boundary element analysis using unstructured t-splines, *Comput. Methods Appl. Mech. Engrg.* 254 (2013) 197–221.
- [21] M.J. Peake, J. Trevelyan, G. Coates, Extended isogeometric boundary element method (XIBEM) for two-dimensional Helmholtz problems, *Comput. Methods Appl. Mech. Engrg.* 259 (2013) 93–102.
- [22] T. Takahashi, T. Matsumoto, An application of fast multipole method to isogeometric boundary element method for Laplace equation in two dimensions, *Eng. Anal. Bound. Elem.* 36 (12) (2012) 1766–1775.
- [23] L. Chen, S. Marburg, W. Zhao, C. Liu, H. Chen, Implementation of isogeometric fast multipole boundary element methods for 2D half-space acoustic scattering problems with absorbing boundary condition, *J. Comput. Acoust.* 27 (02) (2019) 1850024.
- [24] J. Dolz, S. Kurz, S. Schops, F. Wolf, Isogeometric boundary elements in electromagnetism: Rigorous analysis, fast methods, and examples, *SIAM J. Sci. Comput.* 41 (5) (2019) 983–1010.
- [25] M. Bonnet, G. Maier, C. Polizzotto, On symmetric Galerkin boundary element method, *Appl. Mech. Rev.* 51 (1998) 669–704.
- [26] A. Aimi, M. Diligenti, M.L. Sampoli, A. Sestini, Isogeometric analysis and symmetric Galerkin BEM: a 2d numerical study, *Appl. Math. Comput.* 272 (2016) 173–186.
- [27] B.H. Nguyen, H.D. Tran, C. Anitescu, X. Zhuang, T. Rabczuk, An isogeometric symmetric Galerkin boundary element method for two-dimensional crack problems, *Comput. Methods Appl. Mech. Engrg.* 306 (2016) 252–275.
- [28] A. Aimi, F. Calabrò, M. Diligenti, M.L. Sampoli, G. Sangalli, A. Sestini, Efficient assembly based on b-spline tailored quadrature rules for the IgA-SGBEM, *Comput. Methods Appl. Mech. Engrg.* 331 (2018) 327–342.
- [29] X. Peng, E. Atroshchenko, P. Kerfriden, S.P.A. Bordas, Isogeometric boundary element methods for three dimensional static fracture and fatigue crack growth, *Comput. Methods Appl. Mech. Engrg.* 316 (2017) 151–185.
- [30] Y.P. Gong, C.Y. Dong, X.C. Qin, An isogeometric boundary element method for three dimensional potential problems, *J. Comput. Appl. Math.* 313 (2017) 454–468.
- [31] Z. An, T. Yu, T.Q. Bui, C. Wang, N.A. Trinh, Implementation of isogeometric boundary element method for 2-D steady heat transfer analysis, *Adv. Eng. Softw.* 116 (2018) 36–49.
- [32] H. Lian, P. Kerfriden, S.P.A. Bordas, Implementation of regularized isogeometric boundary element methods for gradient-based shape optimization in two-dimensional linear elasticity, *Int. J. Numer. Methods Engrg.* 106 (12) (2016) 972–1017.
- [33] L.L. Chen, H. Lian, Z. Liu, H.B. Chen, E. Atroshchenko, S.P.A. Bordas, Structural shape optimization of three dimensional acoustic problems with isogeometric boundary element methods, *Comput. Methods Appl. Mech. Engrg.* 355 (2019) 926–951.
- [34] F.L. Sun, Y.P. Gong, C.Y. Dong, A novel fast direct solver for 3D elastic inclusion problems with the isogeometric boundary element method, *J. Comput. Appl. Math.* 377 (2020) 112904.
- [35] Y.H. Wu, C.Y. Dong, H.S. Yang, Isogeometric indirect boundary element method for solving the 3D acoustic problems, *J. Comput. Appl. Math.* 363 (2020) 273–299.
- [36] W. Fang, Z.L. An, T.T. Yu, T.Q. Bui, Analysis of unsteady heat transfer problems with complex geometries using isogeometric boundary element method, *CMC-Comput. Mat. Contin.* 62 (2) (2020) 929–962.
- [37] G. Beer, B. Marussig, C. Duenser, *The Isogeometric Boundary Element Method*, Springer, 2020.
- [38] V.P. Nguyen, C. Anitescu, S.P.A. Bordas, T. Rabczuk, Isogeometric analysis: an overview and computer implementation aspects, *Math. Comput. Simulation* 117 (2015) 89–116.

- [39] B. Jüttler, U. Langer, A. Mantzaflaris, S.E. Moore, W. Zulehner, Geometry + simulation modules: Implementing isogeometric analysis, *Proc. Appl. Math. Mech.* 14 (1) (2014) 961–962.
- [40] A.-V. Vuong, Ch. Heinrich, B. Simeon, ISOGAT: a 2D tutorial MATLAB code for isogeometric analysis, *Comput. Aided Geom. Design.* 27 (8) (2010) 644–655.
- [41] C. de Falco, A. Reali, R. Vazquez, GeoPDEs: a research tool for isogeometric analysis of PDEs, *Adv. Eng. Softw.* 42 (12) (2011) 1020–1034.
- [42] D. Rypl, B. Patzak, From the finite element analysis to the isogeometric analysis in an object oriented computing environment, *Adv. Eng. Softw.* 44 (1) (2012) 116–125.
- [43] R.N. Simpson, S.P.A. Bordas, H. Lian, J. Trevelyan, An isogeometric boundary element method for elastostatic analysis: 2D implementation aspects, *Comput. Struct.* 118 (2013) 2–12.
- [44] J. Dölz, H. Harbrecht, S. Kurz, M. Multerer, S. Schöps, F. Wolf, Bembel: The fast isogeometric boundary element c++ library for Laplace, Helmholtz, and electric wave equation, *SoftwareX* 11 (2020) 1–7.
- [45] D. Nardini, C.A. Brebbia, A new approach to free vibration using boundary elements, *Bound. Elem. Methods Engrg.* (1982).
- [46] D. Nardini, C.A. Brebbia, A new approach to free vibration analysis using boundary elements, *Appl. Math. Model.* 7 (3) (1983) 157–162.
- [47] P.W. Partridge, C.A. Brebbia, L.C. Wrobel, *The Dual Reciprocity Boundary Element Method*, Computational Mechanics Publications, Southampton Boston, 1992.
- [48] L.C. Wrobel, C.A. Brebbia, The dual reciprocity boundary element formulation for nonlinear diffusion problems, *Comput. Methods Appl. Mech. Engrg.* 65 (2) (1987) 147–164.
- [49] D.E. Beskos, Boundary element methods in dynamic analysis: Part II (1986–1996), *Appl. Mech. Rev.* 50 (3) (1997) 149–197.
- [50] W.Q. Lu, J. Liu, Y. Zeng, Simulation of the thermal wave propagation in biological tissues by the dual reciprocity boundary element method, *Eng. Anal. Bound. Elem.* 22 (3) (1998) 167–174.
- [51] E.L. Albuquerque, P. Sollero, P. Fedelinski, Dual reciprocity boundary element method in Laplace domain applied to anisotropic dynamic crack problems, *Comput. Struct.* 81 (17) (2003) 1703–1713.
- [52] M.A. Fahmy, Generalized magneto-thermo-viscoelastic problems of rotating functionally graded anisotropic plates by the dual reciprocity boundary element method, *J. Therm. Stresses.* 36 (3) (2013) 284–303.
- [53] B.I. Yun, W.T. Ang, A dual-reciprocity boundary element method for axisymmetric thermoelastostatic analysis of nonhomogeneous materials, *Eng. Anal. Bound. Elem.* 36 (12) (2012) 1776–1786.
- [54] J.H. Zhou, Y.W. Zhang, J.K. Chen, A dual reciprocity boundary element method for photothermal interactions in laser-induced thermotherapy, *Int. J. Heat Mass Transfer* 51 (15–16) (2008) 3869–3881.
- [55] J. Wen, M.M. Khonsari, Transient heat conduction in rolling/sliding components by a dual reciprocity boundary element method, *Int. J. Heat Mass Transfer* 52 (5–6) (2009) 1600–1607.
- [56] B. Yu, H.L. Zhou, H.L. Chen, Y. Tong, Precise time-domain expanding dual reciprocity boundary element method for solving transient heat conduction problems, *Int. J. Heat Mass Transfer.* 91 (2015) 110–118.
- [57] S.P. Guo, X.J. Li, J.M. Zhang, G.F. Bin, W. Huang, A triple reciprocity method in Laplace transform boundary element method for three-dimensional transient heat conduction problems, *Int. J. Heat Mass Transfer* 114 (2017) 258–267.
- [58] K. Chanthawara, S. Kaennakham, W. Toutip, The dual reciprocity boundary element method (DRBEM) with multiquadric radial basis function for coupled burgers' equations, *Int. J. Multiphys.* 8 (2) (2016).
- [59] G. Gomes, A.M.D. Neto, L.M. Bezerra, R. Silva, An object-oriented approach to dual reciprocity boundary element method applied to 2D elastoplastic problems, *Multi. Model. Mat. Str.* 15 (5) (2019) 958–974.
- [60] X.W. Gao, The radial integration method for evaluation of domain integrals with boundary-only discretization, *Eng. Anal. Bound. Elem.* 26 (10) (2002) 905–916.
- [61] E.L. Albuquerque, P. Sollero, W. Portilho de Paiva, The radial integration method applied to dynamic problems of anisotropic plates, *Commun. Numer. Meth. Eng.* 23 (9) (2007) 805–818.
- [62] K. Yang, X.W. Gao, Radial integration BEM for transient heat conduction problems, *Eng. Anal. Bound. Elem.* 34 (6) (2010) 557–563.
- [63] M.A. Al-Jawary, L.C. Wrobel, Radial integration boundary integral and integro-differential equation methods for two-dimensional heat conduction problems with variable coefficients, *Eng. Anal. Bound. Elem.* 36 (5) (2012) 685–695.
- [64] M. Cui, H.F. Peng, B.B. Xu, X.W. Gao, Y.W. Zhang, A new radial integration polygonal boundary element method for solving heat conduction problems, *Int. J. Heat Mass Transfer* 123 (2018) 251–260.
- [65] X.W. Gao, C. Zhang, J. Sladek, V. Sladek, Fracture analysis of functionally graded materials by a BEM, *Compos. Sci. Technol.* 68 (5) (2008) 1209–1215.
- [66] X.W. Gao, B.J. Zheng, K. Yang, C. Zhang, Radial integration BEM for dynamic coupled thermoelastic analysis under thermal shock loading, *Comput. Struct.* 158 (2015) 140–147.
- [67] B. Yu, W.A. Yao, X.W. Gao, S. Zhang, Radial integration BEM for one-phase solidification problems, *Eng. Anal. Bound. Elem.* 39 (2014) 36–43.
- [68] H.S. Carslaw, J.C. Jaeger, *Conduction of Heat in Solids*, second ed., Clarendon Press, Oxford, 1959.
- [69] M. Chasapi, S. Klinkel, A scaled boundary isogeometric formulation for the elasto-plastic analysis of solids in boundary representation, *Comput. Methods Appl. Mech. Engrg.* 333 (2018) 475–496.